Nuclear Engineering and Technology 53 (2021) 532–548

Contents lists available at ScienceDirect

Nuclear Engineering and Technology

journal homepage: www.elsevier.com/locate/net

Original Article

An interactive multiple model method to identify the in-vessel phenomenon of a nuclear plant during a severe accident from the outer wall temperature of the reactor vessel

Anil Kumar Khambampati [a], Kyung Youn Kim [a, **], Seop Hur [b], Sung Joong Kim [c], Jung Taek Kim [b, *]

[a] Department of Electronic Engineering, Jeju National University, South Korea
[b] Research Div. of Autonomous Control, Korea Atomic Energy Research Institute, South Korea
[c] Department of Nuclear Engineering, Hanyang University, South Korea

ARTICLE INFO

Article history:
Received 26 March 2020
Received in revised form
4 August 2020
Accepted 6 August 2020
Available online 20 August 2020

Keywords:
Interactive multiple model
Fault detection
State estimation
Identification of in-vessel phenomena
RV out-wall temperature

ABSTRACT

Nuclear power plants contain several monitoring systems that can identify the in-vessel phenomena of a severe accident (SA). Though a lot of analysis and research is carried out on SA, right from the development of the nuclear industry, not all the possible circumstances are taken into consideration. Therefore, to improve the efficacy of the safety of nuclear power plants, additional analytical studies are needed that can directly monitor severe accident phenomena. This paper presents an interacting multiple model (IMM) based fault detection and diagnosis (FDD) approach for the identification of in-vessel phenomena to provide the accident propagation information using reactor vessel (RV) out-wall temperature distribution during severe accidents in a nuclear power plant. The estimation of wall temperature is treated as a state estimation problem where the time-varying wall temperature is estimated using IMM employing three multiple models for temperature evolution. From the estimated RV out-wall temperature and rate of temperature, the in-vessel phenomena are identified such as core meltdown, corium relocation, reactor vessel damage, reflooding, etc. We tested the proposed method with five different types of SA scenarios and the results show that the proposed method has estimated the outer wall temperature with good accuracy.

1. Introduction

Nuclear power is very necessary to meet the huge energy demands of the future. Moreover, nuclear power can solve the world scale threat of global warming as it produces energy through nuclear fission rather than chemical burning that generates carbon. Nuclear power plants generally contain multiple safety systems, monitoring systems, and sensors that can mitigate and identify several abnormal accident conditions. However, in case of a severe accident, it can lead to damage to nuclear fuel and the vessel, further damaging the containment structures. Consequently, it leads to the release of harmful radioactive gases to the environment [1–3]. In severe accident circumstances, the nuclear facilities are to be designed and operated so that, should a severe accident occur, the facility can be returned to an appropriately safe and stable condition with the radiological consequences mitigated subject to as low as possible. This involves determining the progression of the accident events, their magnitude, and the characteristics of the consequences [1–3].

If the supply of cooling water to the reactor vessel (RV) is not enough or lost, the reactor core remains dry for a considerable time then the temperature of fuel rods rises and can lead to irreversible degradation of the core. The core then starts to melt and then eventually is relocated, typically on a time scale of a few hours at the most. During core degradation, the coolant system of reactor supplies cooling water to the core termed as reflooding a degraded core. In the absence of secondary cooling water, the core gets overheated and then melts. When the hot core flows to the lower head filled with water, it produces steam. This causes a pressure peak or even a steam explosion in the RV, which creates mechanical stresses that are likely to damage the reactor cooling system.

* Corresponding author.
** Corresponding author.
E-mail addresses: kyungyk@jejunu.ac.kr (K.Y. Kim), jtkim@kaeri.re.kr (J.T. Kim).

https://doi.org/10.1016/j.net.2020.08.008

Nomenclature

SA	Severe Accident
IMM	Interacting Multiple Model
FDD	Fault Detection and Diagnosis
RV	Reactor Vessel
CTMT	Containment
KF	Kalman Filter
2-DOF	two-degree-of-freedom
RW	Random-Walk
CV	Constant Velocity
CA	Constant Acceleration
RPV	Reactor Pressure Vessel
OPR-1000	OPR (Optimized power reactor)-1000
SBO	Station Blackout
TLOFW	Total Loss of FeedWater
LOCA	Loss of Coolant Accident
SBLOCA	Small Break Loss of Coolant Accident
MBLOCA	Medium Break Loss of Coolant Accident
LBLOCA	Large Break Loss of Coolant Accident
MFW	Main Feedwater
AFW	Auxiliary Feedwater
Rx	Reactor
SGs	Steam Generators
SITs	Safety Injection Tanks
RCP	Reactor Coolant Pump
x	State variable
n_x	Dimension of State variable
T	Temperature
$\dot{T}$, dT	Rate of Temperature
$\ddot{T}$	Second-order Rate of Temperature
T	Matrix transpose
F	State transition matrix
H	Observation Matrix
Γ	Noise gain Matrix
z_k	Temperature Measurements
P	Error Covariance Matrix
w	Process Noise
v	Measurement Noise
ΔT	Sampling Time
μ	Model probabilities
π	Transition model probabilities
Q	Process noise Covariance
R	Measurement noise Covariance
L	Likelihood function

Besides, the RV exposed to a heat flux that can locally be very high, resulting in erosion of the vessel walls and potentially leading to its failure. The in-vessel phenomena we mainly classify as core exposure, damage to fuel, corium relocation, and reactor vessel damage, failure of CTMT, and radiation release to the outside environment [4–6].

The analysis of severe accident events needs more efficient, independent, and capable methods for safety diagnosis and severe accident management. Fault detection and diagnosis (FDD) have gained a lot of importance recently that assist in the detection of abnormal SA events [7]. The methods for FDD classification include model-based methods and knowledge-based methods [7]. Knowledge-based or data-driven methods are applied when there is a lot of input, output data is available for all scenarios, and knowledge of the system is known instead of an analytical model that describes the process. Knowledge-based or data-driven methods for FDD rely on machine learning and artificial intelligence that include fuzzy systems, neural networks. Moreover, intelligent methods that extract features from prior knowledge and diagnostic expertise are also useful for knowledge-based methods [8–17]. Model-based approaches employ state estimation methods for FDD when there is prior knowledge of the process model. Model-based methods are efficient when an accurate mathematical model is available to describe the process. In SA analysis, there is not much data available for each accident scenario therefore knowledge-based methods are not preferred. Multiple model-based FDD can be used for the estimation of outer wall temperature thus the events can be classified and identified. Kalman filter, which is very popular in the field of target tracking and estimation, can be employed to estimate the unknown wall temperature from the noisy measurement data. Kalman filter uses a single model to describe the behavior of wall temperature, however during a nuclear severe accident, the temperature change is abrupt and complex. Therefore, the state (temperature) that varies continuously in the case of SA cannot be modeled appropriately using a single evolution model. Multiple model (MM) approaches with Kalman filters running in parallel using different evolution models to describe the behavior of the system can be an appropriate method for wall temperature estimation in the SA case. A more recent and efficient method of MM estimation is the interactive multiple model (IMM) method [18–25]. IMM models the unexpected changes in the system by switching probabilistically from one model to another. In IMM based approaches, Kalman filters work in parallel with each model representing a particular fault or features and the residual of each KF defined under a certain threshold are analyzed for the possibilities of faults, and then a decision rule is used to find out which model or fault(s) have occurred.

The objective of this study is to develop an interacting multiple model to classify and identify in-vessel events arising after the severe accident by using the out-wall temperature of the RV. The measured wall temperature from the sensor is contaminated with noise and the evolution of wall temperature is random depending on the SA phenomenon. The noisy temperature data will not give us actual information about SA events, and it is necessary to identify or classify the SA events as early as possible to mitigate the damage. In this work, the estimation of wall temperature is treated as a state estimation problem where the temperature, rate of temperature, and second-order rate of temperature are considered as state variables. The IMM uses a three-parallel bank of Kalman filters operating with three multiple models based on the random-walk and Kinematic models (constant velocity and constant acceleration) to estimate the state variables with good accuracy. From the estimated wall temperature and rate of temperature, it is possible to predict the behavior of wall temperature precisely, and through the estimated wall temperature, the in-vessel phenomenon is identified. In comparison to Kalman filter (KF), IMM is more robust and more accurate in tracking the behavior of wall temperature in SA conditions. We tested the proposed IMM-FDD method with five different severe accident scenarios, and the results show good accuracy in estimating the out-wall temperature.

2. Theory and methodology

2.1. Dynamic state estimation of wall temperature

Let us consider the SA phenomenon and the events occurring

during a severe accident, as illustrated in Fig. 1. To apply interacting multiple model scheme (IMM) for identifying the in-vessel phenomenon, the inverse problem of estimating the wall temperature is treated as a state estimation problem. In the state estimation problem, we need the so-called dynamic model consisting of state equation and observation equation. The state equation consists of a mathematical model that tells about the evolution of state variables, and the observation equation describes the relationship between the state variables and measured values. At first, consider a system where the estimation of the state variable $x \in \Re^{n_x}$, i.e., wall temperature is governed by a linear stochastic difference equation [26,27].

$$x_k = F_{k-1}x_{k-1} + \Gamma_k w_{k-1} \tag{1}$$

with a wall temperature measurement done on the outside of the reactor vessel $z \in \Re^{n_z}$, that is

$$z_k = H_k x_k + v_k, \tag{2}$$

where $F_k \in \Re^{n_x \times n_x}$ is the state transition model, $\Gamma_k \in \Re^{n_x \times n_x}$ is the noise gain model and $H_k \in \Re^{n_z \times n_x}$ is the observation model. The random variables $w_k \in \Re^{n_x}$ and $v_k \in \Re^{n_z}$ denote the process and measurement noises that are assumed to be white Gaussian and independent of each other. Our goal is to set a recursive procedure to estimate state x_k, with the previous states $x_1, \cdots, x_{k-1}$, and the measurements $z_1, \cdots, z_k$. Kalman filter is a popular estimation algorithm that estimates the state x_k from the available measurements.

2.2. Models for wall temperature evolution

In the SA situation, the temperature distribution inside the reactor changes rapidly with time, and therefore it is difficult to describe it mathematically. The Random-walk model which is a simple model can be used to describe the behavior of temperature. A random-walk is a stochastic process described by the two-degree-of-freedom (2-DOF), an analogy of a drunken man taking steps in random directions. The random-walk model assumes that at each time the state variable takes a random step from its previous value, the steps are independently and identically distributed in size. The random-walk process is shown here in a discrete form with w_k representing the unbiased Gaussian white noise

$$x_k = x_{k-1} + w_{k-1} \tag{3}$$

Let us consider the state variables to be estimated are the wall temperature (T), rate of temperature ($\dot{T}$), and second-order rate of temperature ($\ddot{T}$), i.e., $n_x = 3$ and $x_k = [T \quad \dot{T} \quad \ddot{T}]^{\mathrm{T}}$. In the first model for SA identification, let us consider a simple random-walk model, where we estimate temperature alone $x_k = [T \ 0 \ 0]^{\mathrm{T}}$. The measurements available are the outer wall temperature measurement, i.e., the observation matrix has the form $H = [1 \quad 0 \quad 0]$. Using the random-walk model described before, the state transition matrix, noise gain matrix, and observation matrix in the state-space model (1–2) have the form [7,27].

$$F = \begin{bmatrix} 1 & 0 & 0 \\ 0 & 0 & 0 \\ 0 & 0 & 0 \end{bmatrix}, \ \Gamma = \begin{bmatrix} 1 \\ 0 \\ 0 \end{bmatrix}, H = [1 \quad 0 \quad 0] \tag{4}$$

In the next, kinematic models are applied where along with the temperature, the first- and second-order derivatives of temperature are considered as the state variables. Originally, the Kinematic models were developed in the target tracking area [7] to estimate the maneuvering target, in which the acceleration and the jerk are considered as white Gaussian noise for the first- and second-order kinematic models, respectively. Using the Newton's equations of motion, the motion of an object can be represented using velocity and acceleration. Therefore, if the temperature change is linear, it can be considered similar to the case where an object is moving with constant velocity (CV). Assuming, the acceleration term as

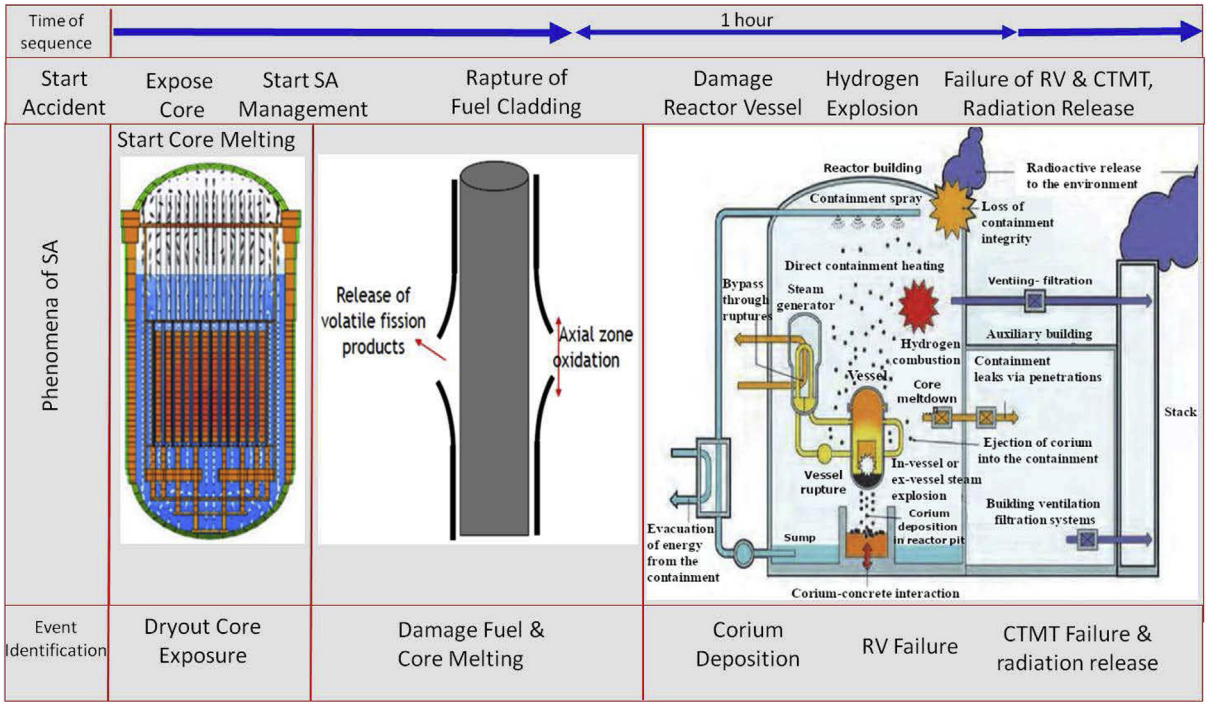

Fig. 1. SA phenomenon and the events occurring during a severe accident.

noise, i.e. $\ddot{T} = w_k$, the equations of motion can be written as

$$T_{k+1} = T_k + \dot{T}_k \Delta T + \frac{1}{2}\Delta T^2 w_k \tag{5}$$

$$\dot{T}_{k+1} = \dot{T}_k + \Delta T w_k \tag{6}$$

$$\ddot{T} = w_k \tag{7}$$

In the CV model, the state variables are the temperature and the rate of temperature $x_k = [T \quad \dot{T} \quad 0]^{\mathrm{T}}$. Using equations (5) and (6), the state transition matrix, noise gain matrix, and observation matrix in the state-space model (1–2) for constant velocity (CV) model has the form [27].

$$F = \begin{bmatrix} 1 & \Delta T & 0 \\ 0 & 1 & 0 \\ 0 & 0 & 0 \end{bmatrix}, \ \Gamma = \begin{bmatrix} \frac{\Delta T^2}{2} \\ \Delta T \\ 0 \end{bmatrix}, H = [1 \quad 0 \quad 0], \tag{8}$$

here ΔT is the time step or sampling interval. And, if the temperature has a nonlinear behavior, then it can be considered similar to the case where the object is moving with constant acceleration (CA). Here, the state variables are the temperature, rate of temperature, and second-order rate of temperature $x_k = [T \quad \dot{T} \quad \ddot{T}]^{\mathrm{T}}$.

Using equations (5)–(7), the state transition matrix, noise gain matrix, and observation matrix in the state-space model (1–2), for constant acceleration (CA) model has the form [27].

$$F = \begin{bmatrix} 1 & \Delta T & \frac{\Delta T^2}{2} \\ 0 & 1 & \Delta T \\ 0 & 0 & 1 \end{bmatrix}, \ \Gamma = \begin{bmatrix} \frac{\Delta T^2}{2} \\ \Delta T \\ 1 \end{bmatrix}, H = [1 \quad 0 \quad 0] \tag{9}$$

The estimation of wall temperature, rate of wall temperature, and second-order rate of the wall temperature would help to understand the change of temperature distribution more efficiently, therefore, it helps to predict the SA events at an earlier time.

2.3. Interactive multiple model algorithm

In the case of a severe accident (SA), the temperature distribution across the reactor vessel (RV) is non-uniform, and the temperature change is abrupt. Therefore, estimation of wall temperature with Kalman filter employing a single model may not give desirable results. In these SA situations, a better state transition model is required other than the random-walk model. Interactive multiple model which uses parallel Kalman filters operating with different state evolution model can be used to have a better estimation of wall temperature. The IMM algorithm is composed of an estimate mixer at the input of each model-conditioned filter, a bank of parallel KF's, a model probability evaluator, and an estimate combiner at the output of the filters. The multiple models interact through the mixing, to estimate the time-varying wall temperature. Considering that the model transition is governed by the Markov chain, the model probabilities and transition probabilities are computed and are used to obtain the mixed estimate for each KF. In the filtering stage, each KF working with a different evolution model uses a mixed estimate and available measurement (wall temperature) to compute a new state estimate. The updated model probabilities are evaluated based on the Likelihood function. Finally, the overall state estimate is computed in the form of the weighted sum of the new estimates and their model probabilities. The IMM algorithm for state estimation of wall temperature is summarized below [28,29].

Step 1. Set the initial conditions for three evolution models $x^i_{0|0}$, $P^i_{0|0}$, μ^i_0, π_{ij}, $F^i (i,j = 1,2,3)$

Step 2. Mixing (interaction) of the estimates.

The mixed initial condition of the jth filter can be computed as.

- mixing estimate

$$x^{0j}_{k|k} = \sum_{i=1}^{3} x^i_{k|k} \mu^{i|j}_k \tag{10}$$

- mixing covariance

$$P^{0j}_{k|k} = \sum_{i=1}^{3} \left[P^i_{k|k} + \left(x^{0j}_{k|k} - x^i_{k|k} \right) \left(x^{0j}_{k|k} - x^i_{k|k} \right)^T \right] \mu^{i|j}_k \tag{11}$$

where $x^{0j}_{k|k}$ and $P^{0j}_{k|k}$ are mixed state and error covariance, respectively. For input of j^{th} model-conditioned KF, model probabilities $\mu^{i|j}_k$ in equations (10) and (11) are defined as

$$\mu^{i|j}_k \equiv \frac{1}{\bar{c}_j} \pi_{ij} \mu^i_k \tag{12}$$

where normalizing constant $\bar{c}_j$ can be calculated by

$$\bar{c}_j = \sum_{i=1}^{3} \pi_{ij} \mu^i_k \tag{13}$$

where π_{ij} is the transition model probability from model i to a model j that is governed by the Markovian process, defined by

$$\pi_{ij} \equiv \Pr\left\{ M^j_{k+1} \middle| M^i_k \right\}, \quad \forall M^i, M^j \in M^s \tag{14}$$

where $\Pr\{\}$ is the probability and M^i_k is the event that the i^{th} mode is in effect at sampling time k, and M^s is the set of all possible model states at all times.

Step 3. Model-conditioned filtering.

Two stages of the model-conditioned KF can be summarized as.

- time update (prediction)

$$x^j_{k+1|k} = F_k x^{0j}_{k|k} \tag{15}$$

$$P^j_{k+1|k} = F_k P^{0j}_{k|k} (F_k)^T + T_k Q^j_k \tag{16}$$

- measurement update (filtering)

$$K^j_{k+1} = P^j_{k+1|k} \left(H^j_{k+1} \right)^T \left(S^j_{k+1} \right)^{-1} \tag{17}$$

$$x^j_{k+1|k+1} = x^j_{k+1|k} + K^j_{k+1} e^j_{k+1} \tag{18}$$

$$P^j_{k+1|k+1} = \left(I^j_{\Lambda} - G^j_{k+1} H^j_{k+1} \right) P^j_{k+1|k} \tag{19}$$

here $G^j_{k+1} \in \mathbb{R}^{\Lambda \times (E+\Lambda)}$ is the Kalman gain at the time $(k+1)T$. The

residuals and their covariances are defined as

$$e^j_{k+1} \equiv z^j_{k+1} - H^j_{k+1} x^j_{k+1|k} \tag{20}$$

$$S^j_{k+1} \equiv H^j_{k+1} P^j_{k+1|k} \left(H^j_{k+1}\right)^T + \Gamma_{k+1} \tag{21}$$

Step 4. Model probability evaluation.

- likelihood function

$$L^j_{k+1} = \frac{1}{\sqrt{2\pi \left| S^j_{k+1} \right|}} \exp\left[-\frac{1}{2} \left(e^j_{k+1}\right)^T \left(S^j_{k+1}\right) e^j_{k+1} \right] \tag{22}$$

- model probability update

$$\mu^j_{k+1} = \frac{1}{c} L^j_{k+1} \bar{c}_j \tag{23}$$

where

$$c = \sum_{i=1}^{N_m} L^i_{k+1} \bar{c}_i \tag{24}$$

Step 5. Combination of estimates.

- overall state estimates

$$x_{k+1|k+1} = \sum_{j=1}^{N_m} x^j_{k+1|k+1} \mu^j_{k+1} \tag{25}$$

- overall error covariance estimate

$$P_{k+1|k+1} = \sum_{j=1}^{N_m} \left[P^j_{k+1|k+1} + \left(x_{k+1|k+1} - x^j_{k+1|k+1} \right) \times \left(x_{k+1|k+1} - x^j_{k+1|k+1} \right)^T \right] \mu^j_{k+1} \tag{26}$$

3. IMM FDD algorithm for the identification of SA events

A fault detection and diagnosis (FDD) algorithm is developed using an interactive multiple model scheme to identify the series of events in a SA scenario. The input data to IMM algorithm is the temperature data from the sensors located along outside the reactor vessel (7 data points). IMM FDD algorithm for temperature starts with an initial guess for temperature, rate of temperature, and second-order rate of temperature and estimates the wall temperature distribution (T). The estimated rate of temperature (dT) enables us to identify the time when the temperature rise or fall is very sharp, thus it can be used to identify events of SA. The IMM FDD scheme for the identification of SAs events is illustrated in the flow diagram given below (Fig. 2).

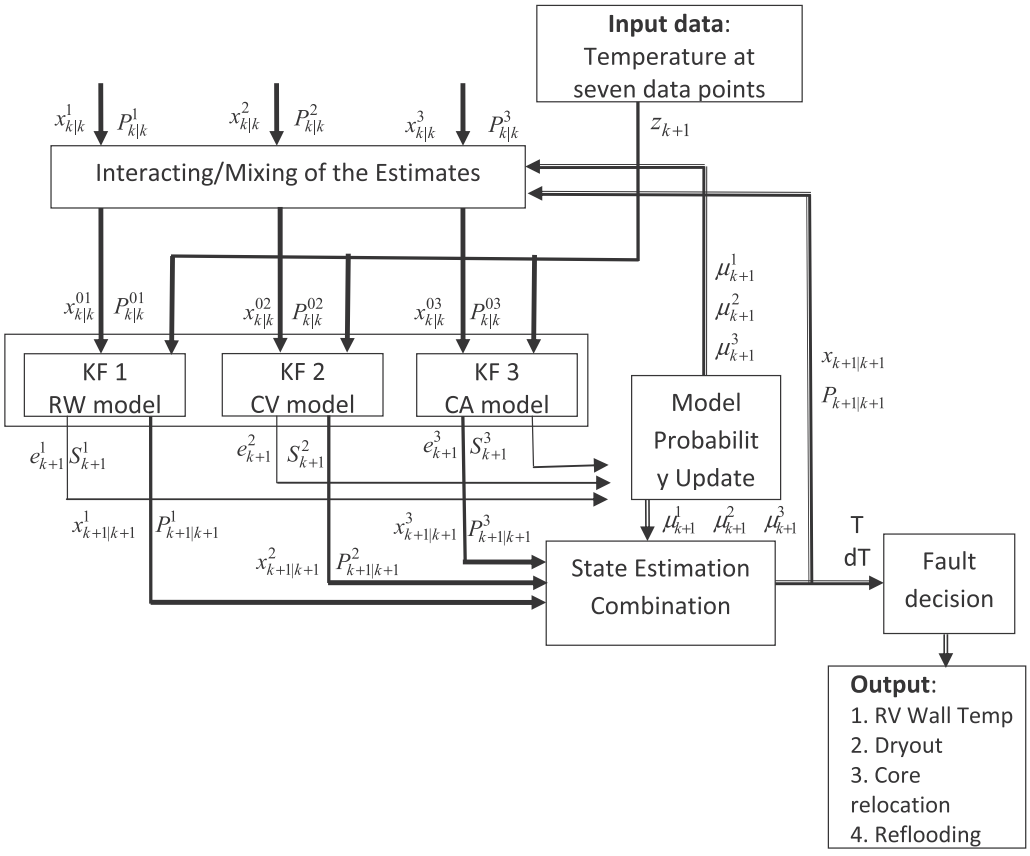

Fig. 2. IMM FDD algorithm for identification of events of SAs using wall temperature.

4. Case study for the identification of in-vessel phenomena using wall temperature

4.1. Computation of wall temperature distribution for SA scenarios

The temperature distribution of inside, outside core, and on the wall outside of the reactor vessel (RV) is simulated for the validation of wall temperature prediction. The MELCOR Code [30] analyzes the phenomenon of severe accidents to estimate the relationship of wall temperature increase, in terms of core temperature. The temperature distribution of the core cell, core baffle, core bypass flow, support barrel, downcomer, wall of reactor pressure vessel (RPV) cylinder, and the lower header is calculated using the MELCOR code. Fig. 3 shows the nodalization used in the MELCOR code for the calculation of temperature distribution across inside, outside core, outer wall of RPV cylinder, and lower header. The design data of OPR(Optimized power reactor)-1000, Korean standard nuclear power plant is used for the simulation of SA scenarios. Two high pressure accidents, such as SBO (Station Blackout), TLOFW (Total Loss of FeedWater) and three low pressure LOCA accidents, such as SBLOCA(Small Break Loss Of Coolant Accident), MBLOCA (Medium Break LOCA) and LBLOCA (Large Break LOCA) are selected as scenarios to simulate the sequence of SAs using the MELCOR code. A small break of 1.35inch on a cold leg is

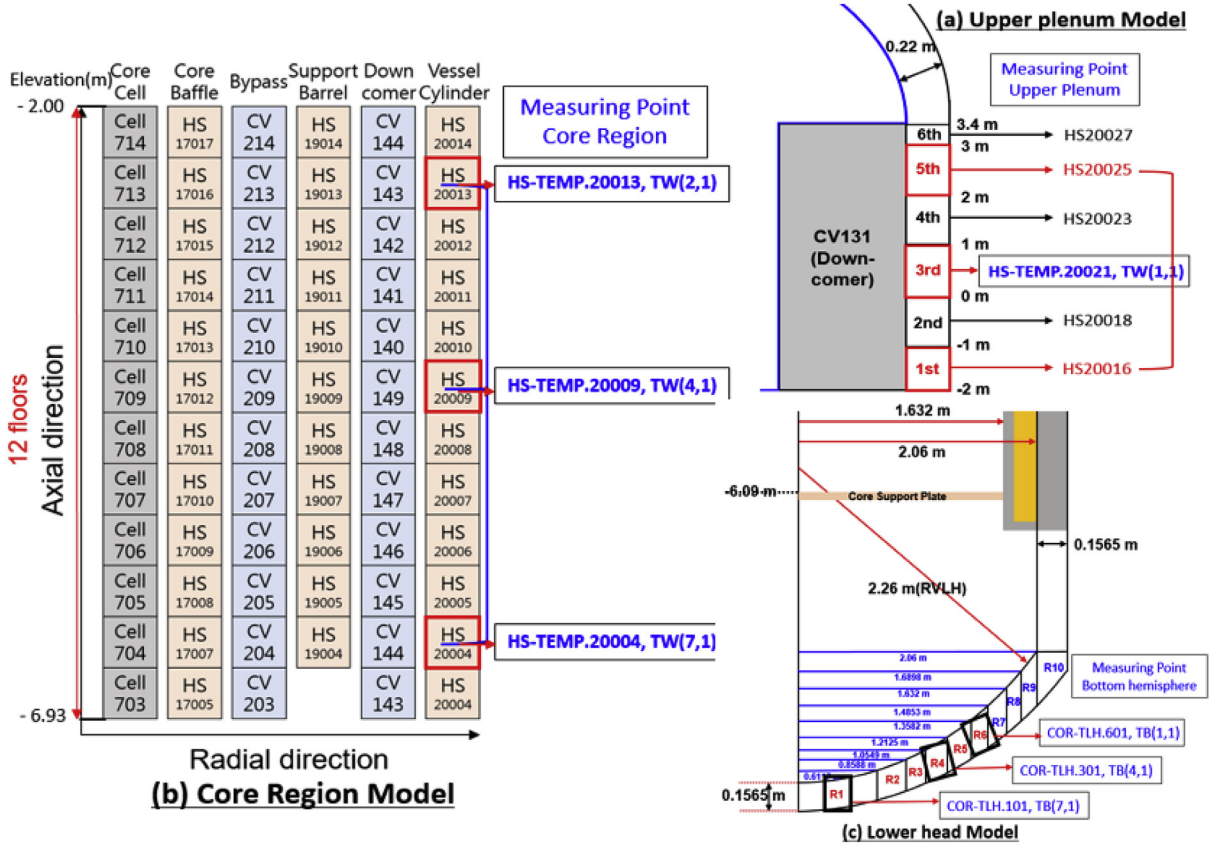

Fig. 3. Nodalization used in the MELCOR code for the calculation of temperature distribution across inside, outside the core, the outer wall of reactor pressure vessel cylinder, and lower header, and seven data points for the temperature calculation and measurement which are placed outside of the RV (a) Upper Plenum (HS-TEMP.20,021, TW (1,1)), (b) Core Region (HS-TEMP.20,013, TW (2,1)), (HS-TEMP.20,009, TW (4,1)), (HS-TEMP.20,004, TW (7,1)), and Lower Header (COR-TLH.601, TB (1.1), COR-TLH.301, TB (4.1), COR-TLH.101, TB (7.1)).

Table 1
The sequence of severe accident scenarios initiated by SBO, TLOFW, SBLOCA, MBLOCA, and LBLOCA.

Sequence of events	Value of actuation	Time [h]				
		Station Black out	TLOFW	SBLOCA	MBLOCA	LBLOCA
RX Trip	RX Trip signal	0	0.01 (28s)	0.04 (148s)	0.01 (18s)	0 (6s)
Trip of RCP	Loss of electric power	0		1.57 (5,659s)		
Dryout of One SG	Mass of H_2O < 1,000 kg	0.95 (3,405s)	0.25 (908s)	3.51 (12,650s)		
Dryout of two SG	Mass of H_2O < 1,000 kg	1.04 (3,731s)	0.25 (900s)			
oxidation of fuel cladding	1,100K	2.59 (9,323s)	1.40 (5,025s)	1.57 (5,659s)	0.99 (3,577s)	0.70 (2,520s)
Dryout of core water level	Water level < −6.09 m	2.97 (10,697s)	1.83 (6,599s)	1.95 (7,037s)	2.67 (9,620s)	0.99 (3,565s)
Melting fuel cladding	2,100K	3.20 (11,522s)	1.80 (6,466s)	1.85 (6,651s)	2.39 (8,591s)	0.89 (3,195s)
Melting fuel and core	2,800K	3.22 (11,580s)	1.84 (6,625s)	1.89 (6,788s)	2.44 (8,784s)	0.94 (3,385s)
Relocation of melting fuel and core	Mass of Relocation Fuel > 0.1 kg	3.24 (11,650s)	1.95 (7,013s)	2.04 (7,338s)	2.79 (10,053s)	1.49 (5,352s)
Failure of RPV	Temp of penetration pipe > 1,273K	6.77 (24,358s)	4.90 (17,647s)	12.95 (46,632s)	4.07 (14,656s)	2.72 (9,787s)
Injection from SIT	Pressure of RV < 4.3 MPa	6.83 (24,575s)	4.96 (17,868s)	2.61 (9,392s)	0.28 (1,017s)	0.08 (287s)
Exhaustion of SIT	Level of SIT < 6.21 m	7.11 (25,596s)	5.25 (18,889s)	12.99 (46,770s)	1.30 (4,697s)	0.22 (777s)

assumed as the base case of SBLOCA. For the SBO base case, the off-site power is assumed to be lost. For the TLOFW base case, main feedwater (MFW) and auxiliary feedwater (AFW) are considered unavailable. Table 1 shows the sequence of severe accident scenarios, such as SBO, TLOFW, SBLOCA, MBLOCA, and LBLOCA initiated accidents.

During the severe accident scenarios, after the Rx Trip occurs, SGs (Steam Generators) get dried out, and the fuel assemblies of the RV are exposed as the water level decreases. The temperature of fuel cladding increases to 1,100K, and then the oxidation of fuel cladding occurs. The temperature of core and fuel increases rapidly and then accelerates to the melting temperature of the fuel. And so, the wall temperature of the RV increases continuously. Corium, the melted fuel, comes down to the lower header, i.e., the bottom hemisphere of the RV, and so the wall temperature of the bottom hemisphere of the RV increases abruptly. Furthermore, when the

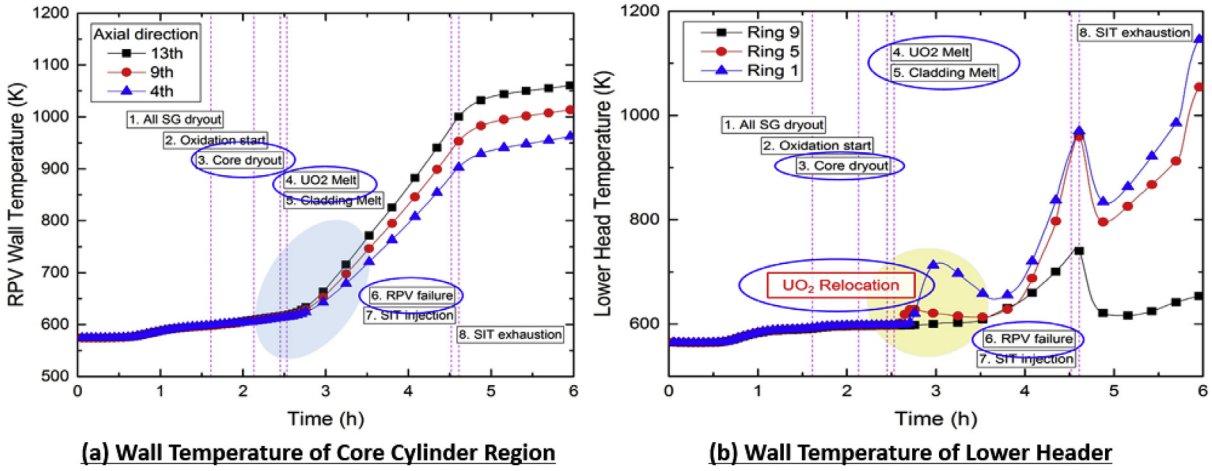

Fig. 4. Distribution of wall temperature of cylinder and lower header of RPV bottom hemisphere, as an example for a sequence of in-vessel phenomena after severe accident scenario initiated by SBO.

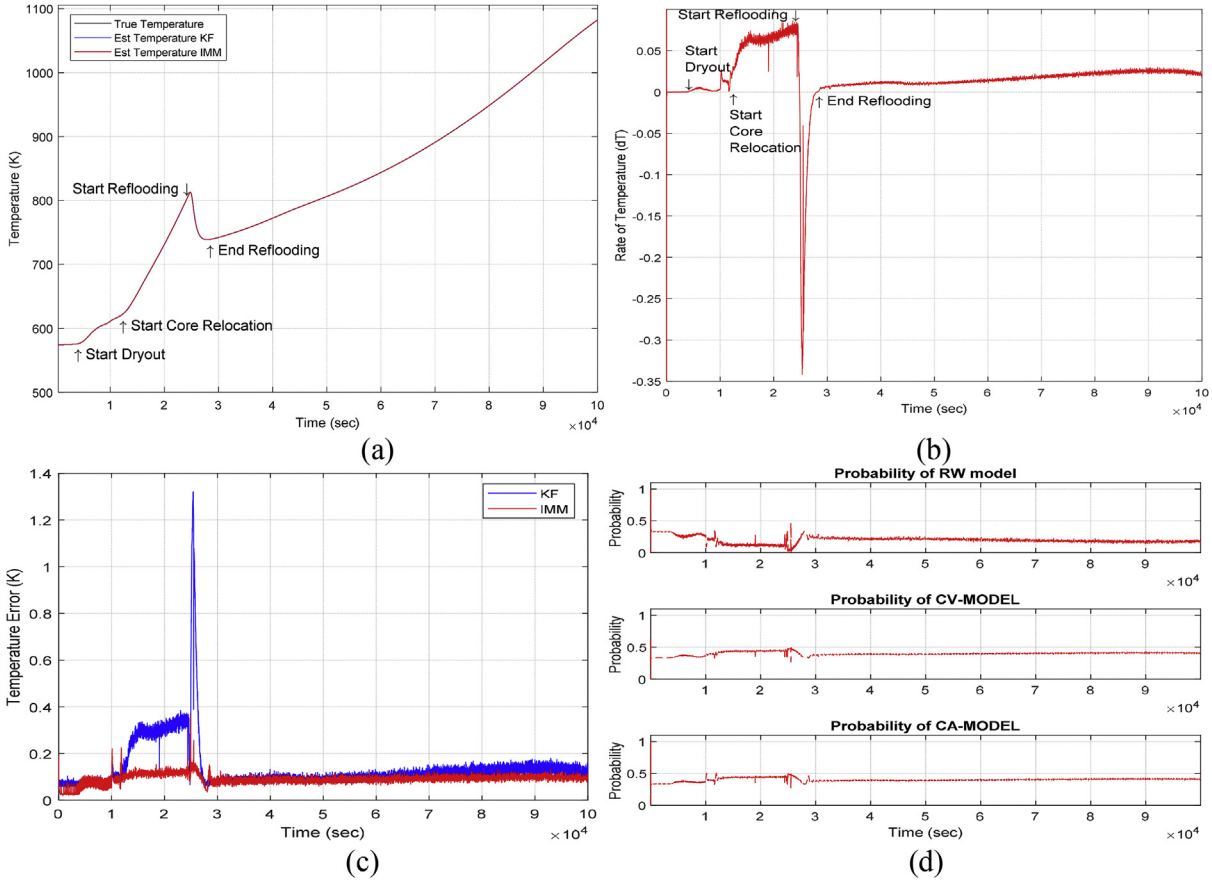

Fig. 5. Results for wall temperature estimation in SBO scenario for data point 4 (HS-TEMP.2,000,404) (a) estimated outer wall temperature using KF and IMM (b) estimated rate of temperature with IMM (c) temperature estimation error (d) model probabilities.

wall temperature of the lower header reaches 1,273K, then eventually the failure of RPV starts. After that, the pressure of the RV decreases to 4.3 MPa, and then the cooling water is injected into the RV from SITs (safety injection tanks). The temperature of the RV then decreases while the injected cooling water is dried out. As the cooling water is dried out, the temperature of the lower header and wall of the RV again increases rapidly. Fig. 4 shows the distribution of wall temperature of RPV cylinder and lower header of RPV bottom hemisphere, as an example for the sequence of in-vessel phenomena after a severe accident scenario initiated by SBO.

The simulation data of the wall temperature of the RV and the lower header is available from the calculated results of the seven data points, placed outside of the reactor for the sequence of events that occur from different severe accident scenarios as shown in

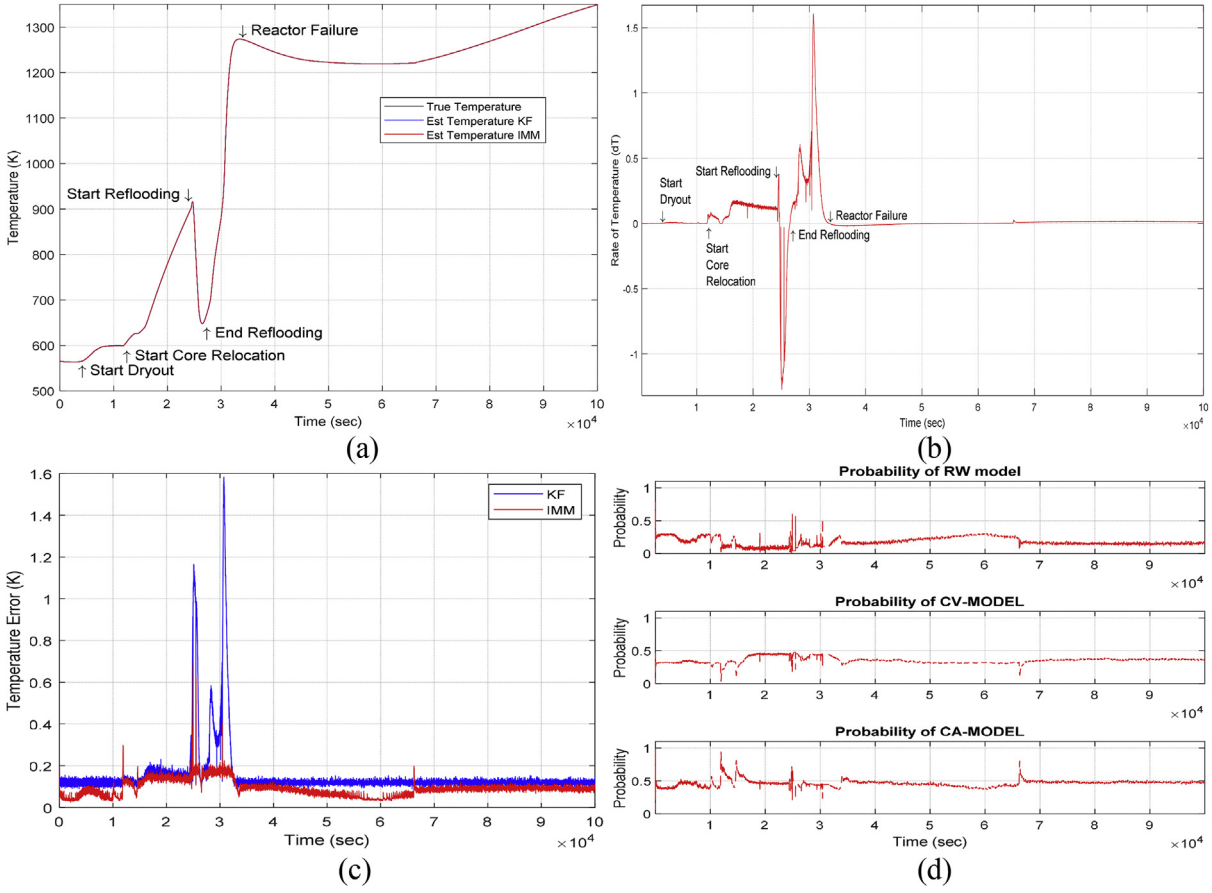

Fig. 6. Results for wall temperature estimation in SBO scenario for data point 6 (COR-TLH.301) (a) estimated outer wall temperature using KF and IMM (b) estimated rate of temperature with IMM (c) temperature estimation error (d) model probabilities.

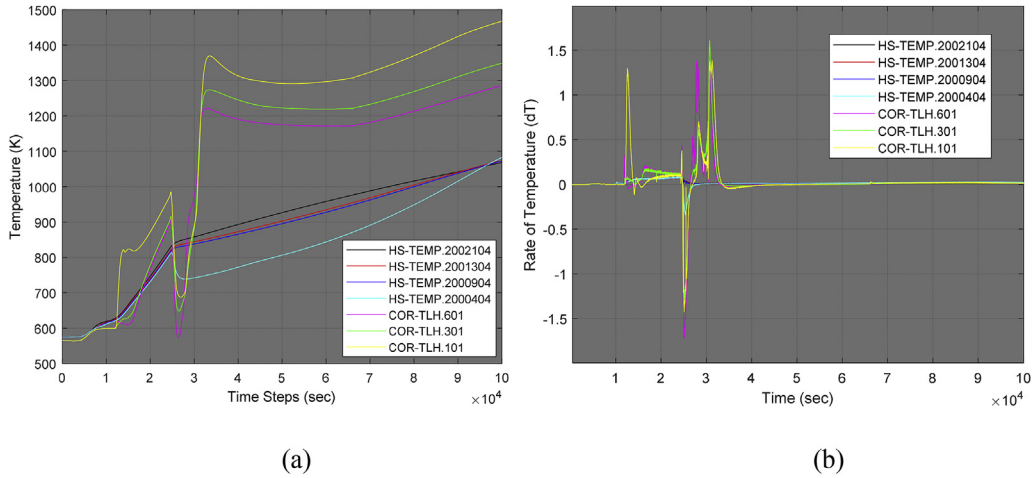

Fig. 7. Results for wall temperature estimation for all seven data points in SBO scenario (a) estimated outer wall temperature using IMM at different locations of the reactor (b) estimated rate of temperature.

Fig. 3. Locations for the data points for temperature measurement are RX Vessel Upper Plenum 1 Point (TW (1,1) HS-TEMP.20,021), RX Vessel Core Wall 3 Points (TW (2,1) HS-TEMP.20,013), (TW (4,1) HS-TEMP.20,009), (TW (7,1) HS-TEMP.20,004)), and Bottom hemisphere three points (TB (1,1) COR-TLH.601), (TB (4,1) COR-TLH.301), (TB (7,1) COR-TLH.101). The data for temperature is available for five different SA simulation scenarios, mainly SBO, TLOFW, SBLOCA, MBLOCA, and LBLOCA, respectively.

4.2. Numerical simulation for wall temperature estimation

The simulated temperature data from seven data points are labeled as HS-TEMP2002104, HS-TEMP.2,001,304, HS-TEMP.2,000,904, HS-TEMP.2,000,404, COR-TLH.601, COR-TLH.301, COR-TLH.101, respectively. The true temperature data is then added with random white Gaussian noise of standard deviation 0.1 to account for the instrument and environment errors. To analyze and identify the sequence of events using IMM and KF, for five SA scenarios, two data points are selected. The chosen two data points are HS-TEMP.2,000,404 that corresponds to the lower position of the reactor core, and COR-TLH.301, the data point located at the bottom middle hemisphere of the RV. In the implementation of IMM for temperature estimation, the Markov transition probabilities π_{ij} are assigned as 0.9 for $i = j$ and 0.05 for $i \neq j$ and the initial model probabilities $(\mu_0^i,\ i = 1,2,3)$ were set to be $\frac{1}{3}$. The initial condition for temperature, rate of temperature and second order rate of temperature for IMM and KF for all the cases is considered as $x_{0|0} = [300, 0.5, 0.5]^{\mathrm{T}}$. The error covariance matrix is assumed as 100 and the process ment noise covariance are set in the range of 1e-10 for all the cases. The measurement noise covariance is assumed in the range 1e-8 to 5e-10 for KF and 1e-2 to 5e-2 in the case of IMM.

4.2.1. Results for SBO scenario

The estimation results of wall temperature for SA scenario SBO with IMM and KF, for data points HS-TEMP.2,000,404 and COR-TLH.301 are shown in Fig. 5 and Fig. 6, respectively. The estimation of wall temperature at the reactor core (HS-TEMP.2,000,404) is shown in Fig. 5(a) and the rate of temperature (dT) is shown in Fig. 5(b). In Fig. 5(a), it is noticed that the wall temperature increases continuously after 3,400sec. The rate of temperature change is observed to be more rapid after 11,711sec, and an increase of 190K is observed during the next 13,000sec. Then, the temperature drops by around 74 K, and subsequently the temperature is found to increase continuously to near about 1082 K in 99,990sec. The slope of the dT plot shown in Fig. 5(b) gives a better illustration of the wall temperature variation. The positive dT value suggests there is an increase in wall temperature and negative value suggests there is a decrease in wall temperature. Using the T and dT plots of Fig. 5(a and b), it is possible to identify the sequence of SA events. The initial rise in the temperature around 3,400sec indicate the start of dryout condition, and at 11,711sec there is a rapid increase in wall temperature that points to the start of core relocation, i.e., melting of fuel corium. Furthermore, RV wall temperature reduces continuously for a period after 24,780sec due to the injection of cooling water, which is identified as the start of reflooding. The wall temperature increases again continuously after

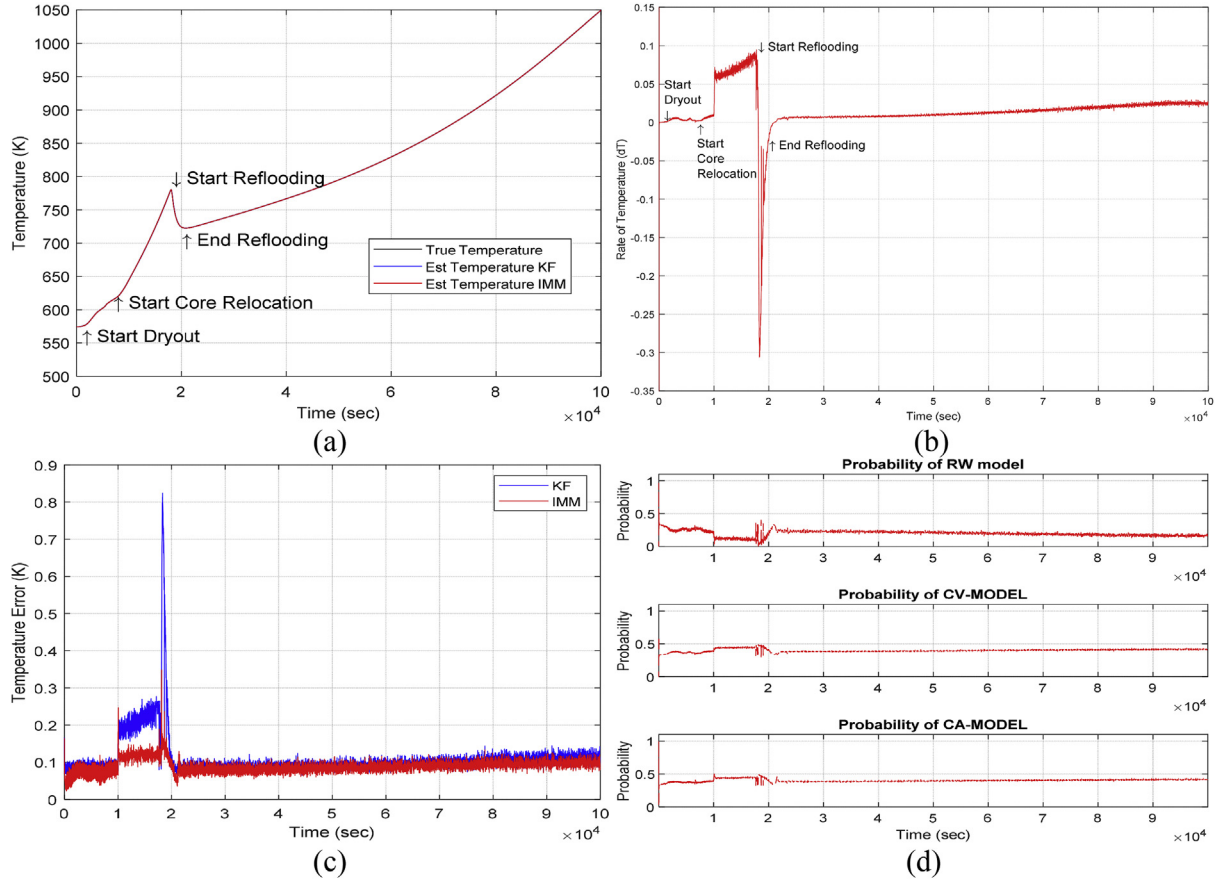

Fig. 8. Results for wall temperature estimation in TLOFW scenario for data point 4 (HS-TEMP.2,000,404) (a) estimated outer wall temperature using KF and IMM (b) estimated rate of temperature with IMM (c) temperature estimation error (d) model probabilities.

27,820sec signaling the end of reflooding. The difference between the axial temperature of the top, middle, and bottom position of RV is not much in terms of the sequence of severe accident scenarios. But, it can be identified that the axial temperatures of the top, middle, and bottom position of RV is rapidly increasing or decreasing at the start of dryout condition, the start of core relocation, and the start of reflooding. The temperature estimation error with IMM and KF is shown in Fig. 5(c). And, as noticed, IMM has better estimation performance of wall temperature as compared to KF when the temperature of RV due to SA changes abruptly and has nonlinear or linear behavior. The model probabilities for each model used in the IMM is shown in Fig. 5(d). From Fig. 5(d), the CV and CA models have higher model probabilities values as compared to the random-walk model when the change in wall temperature is linear or nonlinear.

Fig. 6 shows the estimation result of wall temperature

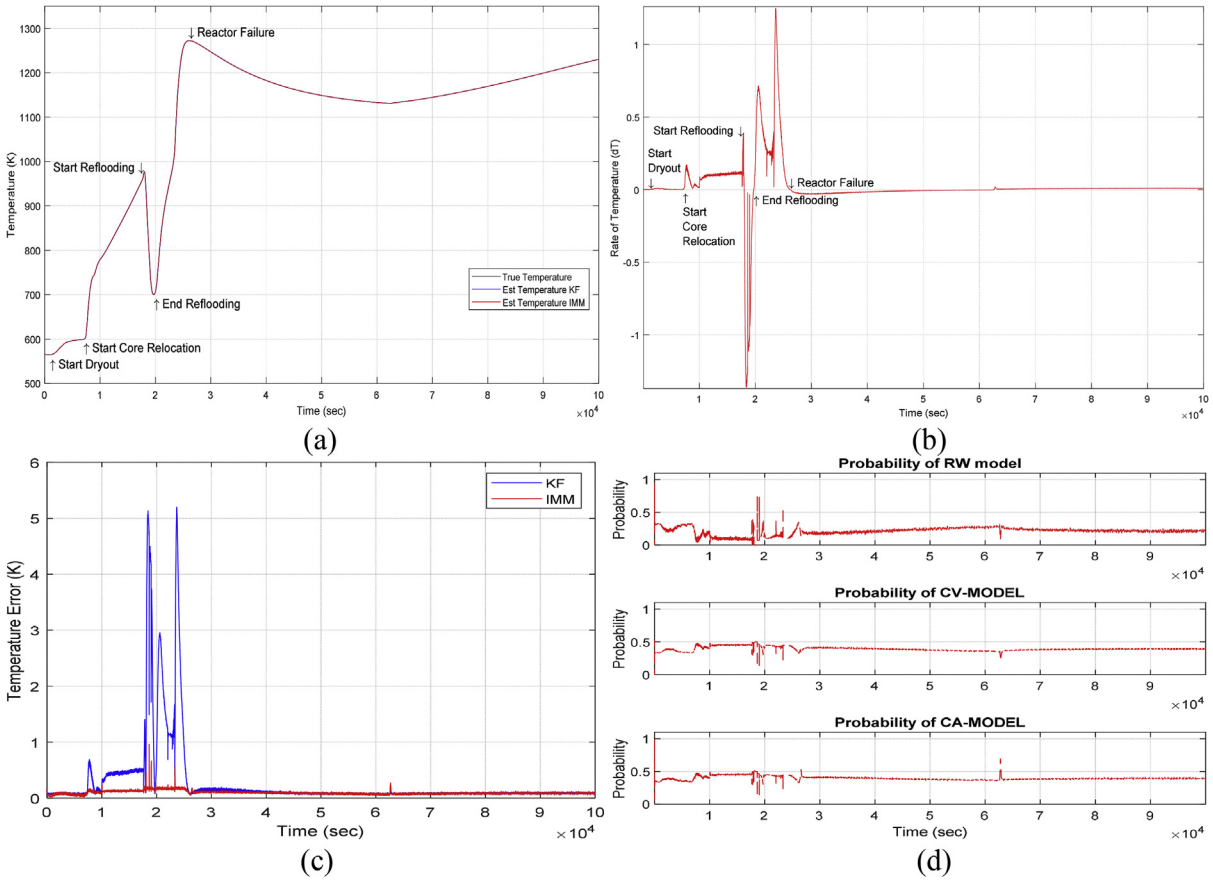

Fig. 9. Results for wall temperature estimation in TLOFW scenario for data point 6 (COR-TLH.301) (a) estimated outer wall temperature using KF and IMM (b) estimated rate of temperature with IMM (c) temperature estimation error (d) model probabilities.

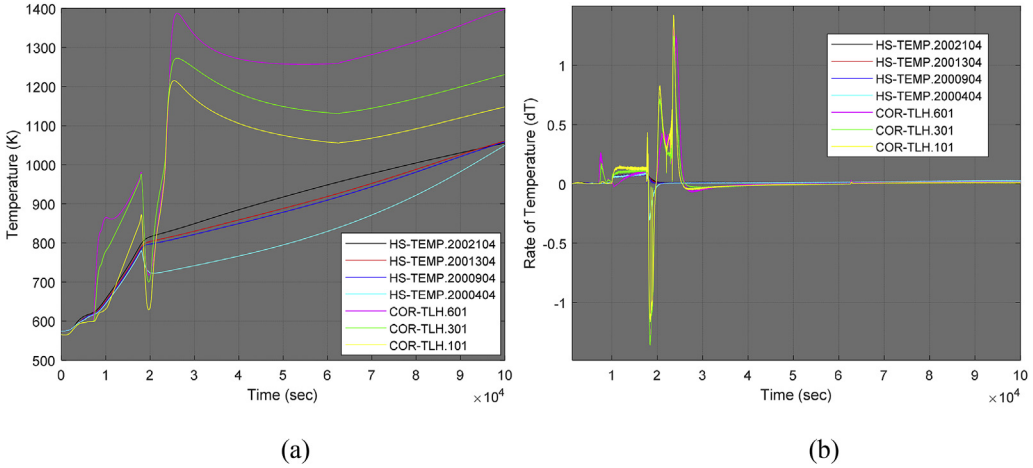

Fig. 10. Results for wall temperature estimation at all seven data points in TLOFW scenario (a) estimated outer wall temperature using IMM at different locations of the reactor (b) estimated rate of temperature.

distribution for the RV bottom hemisphere data point COR-TLH.301. The wall temperature is estimated with good accuracy by IMM and KF (Fig. 6(a)). However, the estimation error with single model KF is large as compared to IMM when the temperature change due to SA events is abrupt (Fig. 6(c)). The *dT* plot (Fig. 6(b)) shows the estimated rate of temperature and as compared to data point HS-TEMP.2,000,404, the *dT* curve of COR-TLH.301 has a higher slope and magnitude. From *T* and *dT* plots, after the time 3,450sec, a sudden increase in wall temperature is noticed which is labeled as dryout condition, and at time 11,651sec, a positive spike is observed in the *dT* plot that is identified as the start of core relocation. Further, the negative slope of the *dT* curve at time 24,580sec indicates a decrease in the wall temperature suggesting the start of reflooding. After the cooling water dried out, the wall temperature again starts to rise after 26,630sec, which is termed as the end of reflooding. After the reflooding ends, the RV temperature rises rapidly and at 33,250sec, due to a very high temperature, the reactor reaches a critical stage causing reactor failure. Afterward, the wall temperature decreases for a short period and again increases continuously. The model probabilities for each KF model used in the IMM for wall temperature estimation are shown in Fig. 6(d). Fig. 7 shows the IMM estimation results of *T* and *dT* for all of the seven data points in the SBO SA scenario. The wall temperature at the bottom hemisphere of the RV has a greater fluctuation as compared to the reactor core area and Upper Plenum. Also, the sequence of SA events such as dryout, core relocation, cooling water injection, and reflooding for the bottom hemisphere data points appear before as compared to the data points on reactor core and upper plenum.

4.2.2. Results for TLOFW scenario

In the next SA scenario TLOFW, the results for the estimation of the wall temperature are reported in Fig. 8 and Fig. 9, for the data points HS-TEMP.2,000,404 and COR-TLH.301, respectively. From Fig. 8, due to the lack of supply of main feedwater and auxiliary feedwater on the secondary side, the wall temperature increases rapidly. At 1,000sec, there is a sharp rise in the estimated wall temperature that signals the start of dryout condition, and around 7,018sec the rate of temperature further increases indicating the start of core relocation. After that, the wall temperature increases to an alarming level of 890K, therefore cooling water is introduced at 18,000sec, which suggests the start of the reflooding event. Subsequently, after the reflooding is ended at 20,071sec, the temperature inside the reactor is found to increase again continuously until 1,050K. The temperature error and model probabilities associated with each model in IMM for temperature estimation is shown in Fig. 8(c and d). IMM has a better estimation of wall temperature as compared to KF and it is noticed that when the temperature change has a linear or nonlinear behavior, the CV and CA model are dominant as compared to the RW model.

The wall temperature estimation using IMM and KF for the bottom hemisphere data point COR-TLH.301 is shown in Fig. 9. From the estimated wall temperature and rate of temperature plots (Fig. 9(a and b)), the SA events are identified and classified as follows. The wall temperature is stable until 922sec, and the lack of feedwater causes a rise in the wall temperature, which is termed as the start of dryout condition. An increase in the slope of the estimated rate of temperature around 7,028sec can be identified as the start of core relocation. The temperature rises sharply after the core

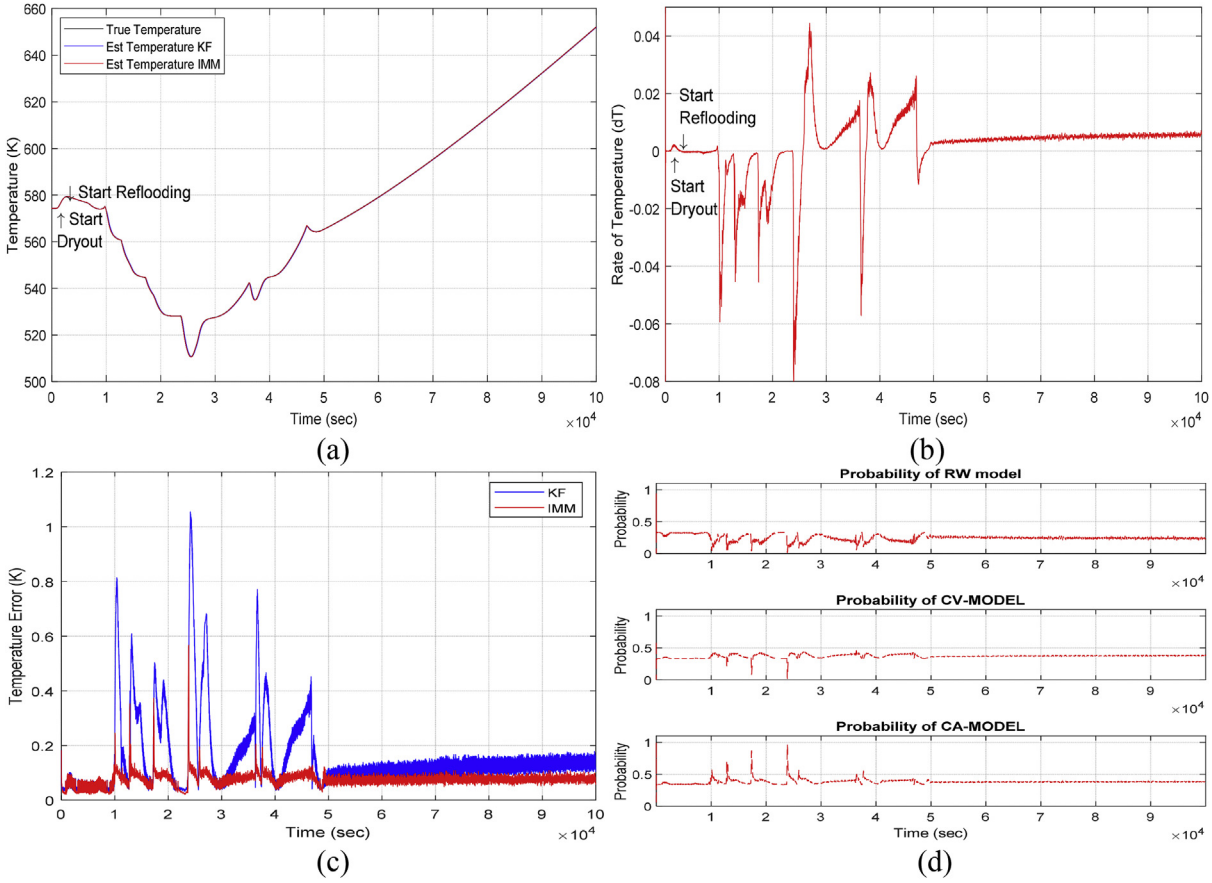

Fig. 11. Results for wall temperature estimation in SBLOCA scenario for data point 4 (HS-TEMP.2,000,404) (a) estimated outer wall temperature using KF and IMM (b) estimated rate of temperature with IMM (c) temperature estimation error (d) model probabilities.

relocation occurred thus bringing the overall core temperature close to 890K. Due to the injection of cooling water at 18,070 s, termed as reflooding, the estimated wall temperature decreases, i.e., the dT curve has a negative slope at 18,070sec. After the reflooding ends at 19,689sec, the estimated wall temperature increases rapidly to 1280K, and the rate of temperature has a maximum value, leading to reactor failure. The wall temperature then drops for a while after the reactor failure, and again it increases continuously. The temperature estimation error and model probabilities of IMM for temperature distribution are shown in Fig. 9(c and d). Overall, it is found that IMM has better wall temperature estimates as compared to KF.

Wall temperature plots and rate of temperature plots for the TLOFW scenario at all seven data points are shown in Fig. 10. As seen from Fig. 10(a), the sequence of events in the TLOFW scenario, such as dryout, core relocation, cooling water injection, and

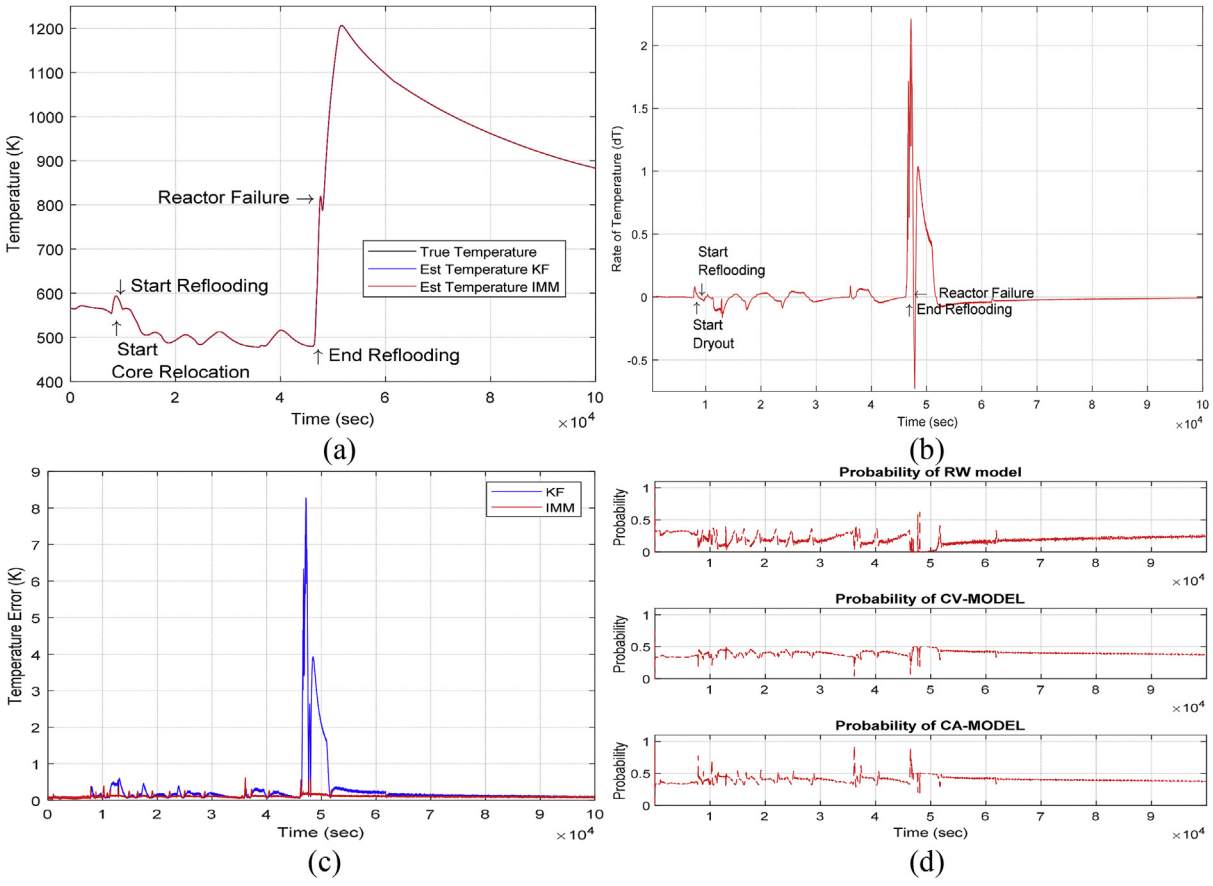

Fig. 12. Results for wall temperature estimation in SBLOCA scenario for data point 6 (COR-TLH.301) (a) estimated outer wall temperature using KF and IMM (b) estimated rate of temperature with IMM (c) temperature estimation error (d) model probabilities.

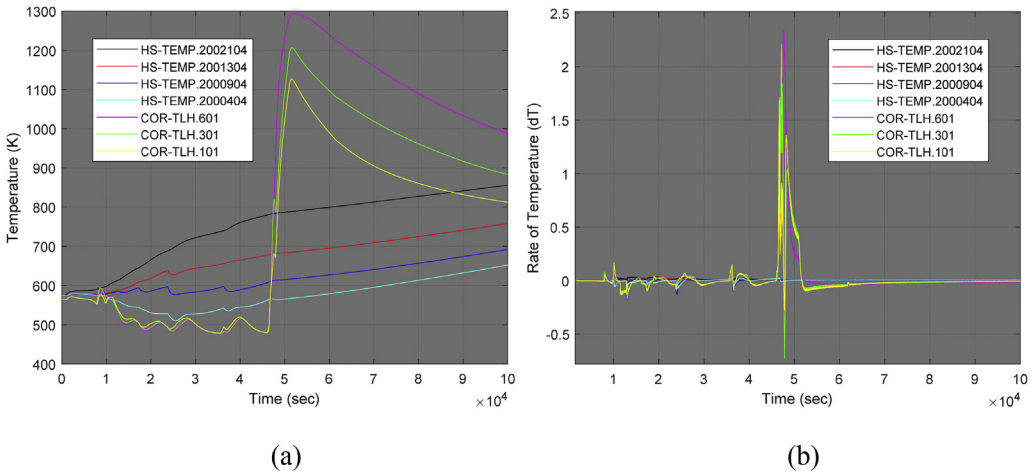

Fig. 13. Results for wall temperature estimation at all seven data points in SBLOCA scenario (a) estimated outer wall temperature using IMM at different locations of the reactor (b) estimated rate of temperature.

reflooding for the bottom hemisphere data points occurred early as compared to the data points on the reactor core and upper plenum. Moreover, the *dT* slope for the bottom hemisphere has more magnitude that signifies the temperature change is more rapid. Furthermore, the start of core relocation in the lower hemisphere data point, COR-TLH.601, has occurred early, as compared to the other data points located on the outer wall.

4.2.3. Results for SBLOCA scenario

In the next SA scenario, we have SBLOCA results for wall temperature estimation. Fig. 11 and Fig. 12 has the result for wall temperature estimation for data point at HS-TEMP.2,000,404 and COR-TLH.301. In the case of HS-TEMP.2,000,404 (Fig. 11), the temperature change is not very high as compared to other SA cases, such as SBO and TLOFW. The wall temperature is found to be stable until the dryout of SG (Steam Generator) occurs, and a decrease in temperature is observed which can be attributed due to the injection of cooling water. The estimated wall temperature decreases to 510K at 25,530sec, and then it increases again as a result of the exhaustion of cooling water. The water level goes below the 4th data point (−6.09 m), resulting in a steady increase of the wall temperature from 510K to 651K. The difference in the wall temperature between the top, middle, and bottom of the RV core is very high and has a different trend, as compared to SBO and TLOFW scenarios. Moreover, in the case of HS-TEMP.2,000,404, we could identify only the starting time of the dryout condition of SG and cooling water injection. The estimation error of wall temperature is shown in Figure(11(c)), and IMM has a lower estimation error as compared to KF. The model probabilities used in IMM for the estimation of temperature are shown in Fig. 11(d). As noticed, when there is a sudden drop in wall temperature, the CA model is dominant, and if the change in wall temperature is steady, then a combination of CA and CV model is used to estimate the wall temperature.

In the case of COR-TLH.301 (Fig. 12(a and b)), the estimated temperature is stable or decreasing at the beginning of SBLOCA SA. The estimated wall temperature starts to rise after 7,782sec, and at this instant, the *dT* curve has a greater magnitude, which indicates the start of core relocation. Cooling water is injected after 8,646sec, for discharging steam through the cold-leg small break. The estimated wall temperature decreases gradually until the cooling water injection exhausts at 46,271sec. After that, the wall temperature starts to rise continuously up to 1,200K, and the reactor failure occurs at 47,621sec, as seen in Fig. 12(a). The *dT* plot in Fig. 12(b) at 47,621 s has a huge spike that notifies the rapid rise in temperature to a critical point. In the case of COR-TLH.301, we identify the SA events such as the starting time of core relocation, cooling water injection, exhausting time of cooling water, and RPV failure.

The temperature and rate of temperature plots for the SBLOCA scenario at all seven data points are plotted in Fig. 13. As seen from Fig. 13(a), the sequence of events in the SBLOCA scenario, such as dryout, core relocation, cooling water injection, and reflooding, for the bottom hemisphere data points, appear early, as compared to the data points on reactor core and upper plenum. Moreover, the *dT* slope for the bottom hemisphere has more magnitude that signifies the temperature change is more rapid, and the SA events initiated early at datapoint COR-TLH.101 compared to other data points.

4.2.4. Results for MBLOCA scenario

In the case of the MBLOCA scenario, the water level of the RV

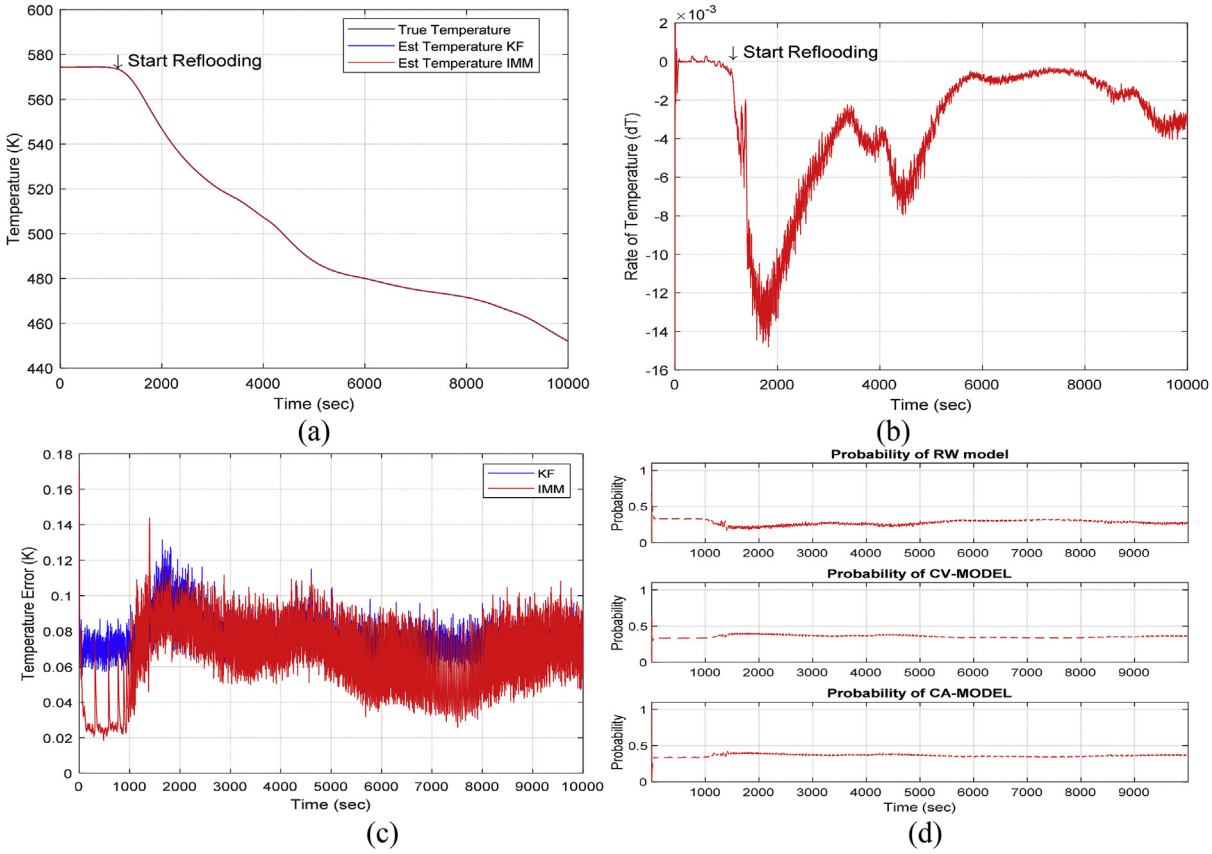

Fig. 14. Results for wall temperature estimation in MBLOCA scenario for data point 4 (HS-TEMP.2,000,404) (a) estimated outer wall temperature using KF and IMM (b) estimated rate of temperature with IMM (c) temperature estimation error (d) model probabilities.

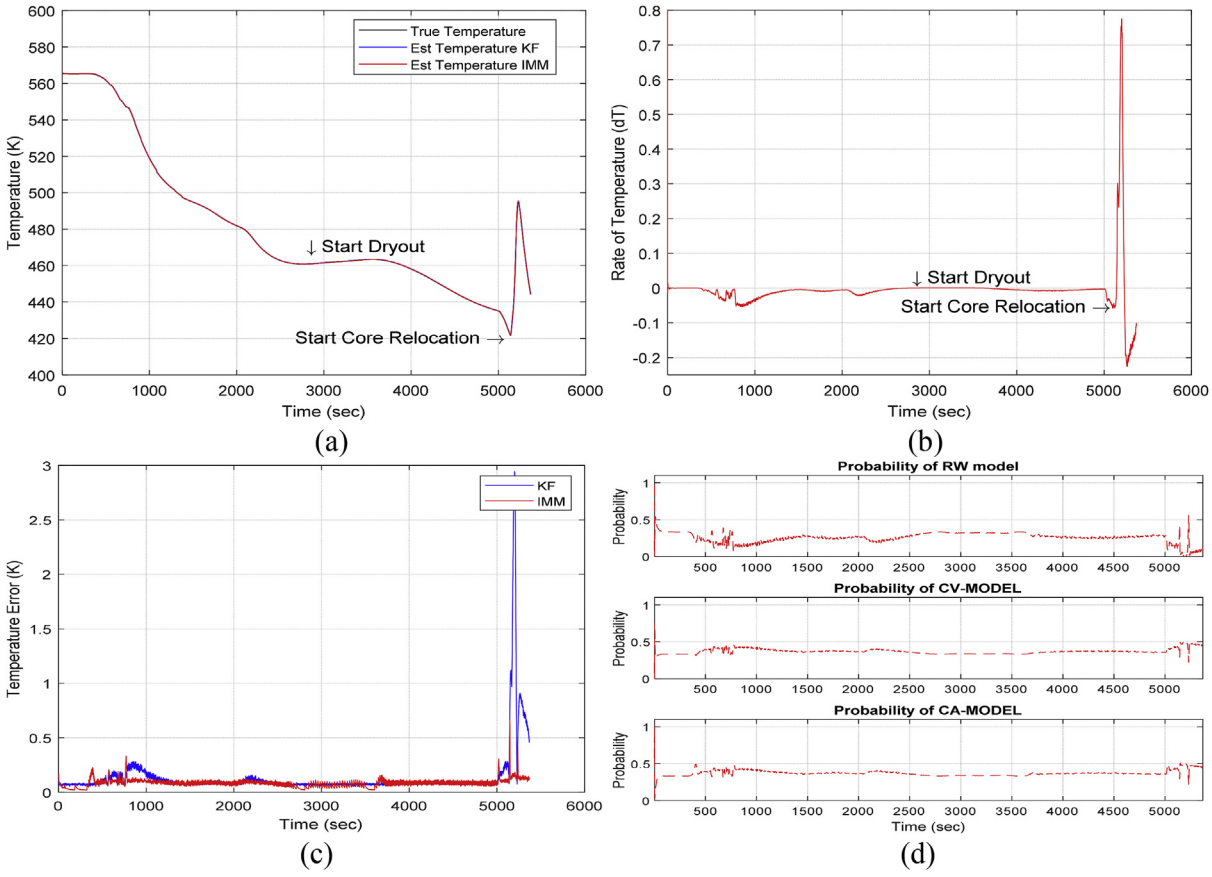

Fig. 15. Results for wall temperature estimation in MBLOCA scenario for data point 6 (COR-TLH.301) (a) estimated outer wall temperature using KF and IMM (b) estimated rate of temperature with IMM (c) temperature estimation error (d) model probabilities.

quickly decreases as compared to the SBLOCA scenario because the break size is large, and the coolant in the RV discharges quickly through the location of the break. Fig. 14 displays the results for wall temperature estimation for data point at HS-TEMP.2,000,404. The estimated wall temperature is stable, and after the cooling water is injected at 1,052sec, the temperature decreases continuously (Fig. 14(a)). After 1,052sec, it is observed that the rate of temperature (dT) is negative until the end of the operation (Fig. 14(b)).

In COR-TLH.301, for MBLOCA, the estimated wall temperature is stable before the injection of cooling water at 400sec. The wall temperature then decreases continuously until the dryout of cooling water occurred at 2,800sec. As seen from Fig. 15, after the dryout of cooling water, the wall temperature is stable because most of the steam heat source is released outside the RV, and the melted fuel debris finally comes down to the bottom hemisphere.

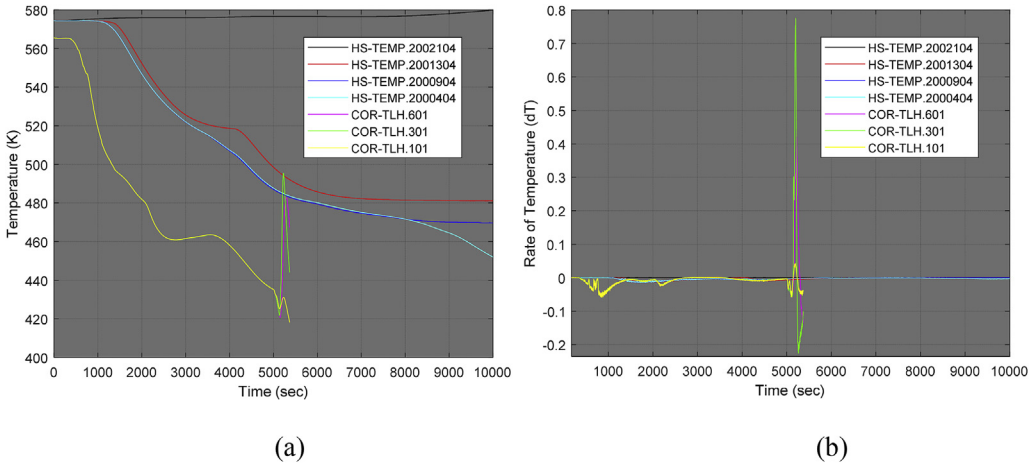

Fig. 16. Results for wall temperature estimation at all seven data points in MBLOCA scenario (a) estimated outer wall temperature using IMM at different locations of the reactor (b) estimated rate of temperature.

Finally, the wall temperature increases after 5,139sec, and here the core relocation is initiated.

The Temperature plots and the rate of temperature plots for the MBLOCA scenario for all seven data points are shown in Fig. 16. For MBLOCA, except for the lower hemisphere data points, the estimated wall temperature is less than 500K, for a longer period. As seen from Fig. 16(a), the sequence of SA events of MBLOCA scenario, such as cooling water injection, dryout of cooling water, and core relocation for the bottom hemisphere data point, COR-TLH.101 is initiated ahead as compared to the data points on the reactor core and upper plenum. Moreover, the *dT* slope for bottom hemisphere data points has more magnitude that signifies the temperature change is more rapid.

4.2.5. Results for LBLOCA scenario

In the case of the LBLOCA scenario, the progression of in-vessel phenomena is very fast as compared to the MBLOCA and the SBLOCA scenarios. Due to the large break size, the coolant in RV gets released quickly through the point of the break. Fig. 17 and Fig. 18 has the wall temperature estimation result for data points at HS-TEMP.2,000,404 and COR-TLH.301. In the case of the LBLOCA scenario, for the data point at HS-TEMP.2,000,404 (Fig. 17), the estimated wall temperature is stable in the beginning, and after 352sec, the temperature is found to decrease due to the injection of cooling water. Cooling water is dried out at 7902 s and thus causing a rapid rise in the estimated wall temperature until the RPV failure occurs.

But, in the case of COR-TLH.301 (Fig. 18), the estimated wall temperature is steady until 272sec, and with the inclusion of cooling water immediately after the reactor trip, it causes a decrease in the estimated wall temperature. The estimated wall temperature rises again after 5,462sec once the cooling water gets dried up, which can be considered as the starting time of relocation of melting fuel and core. The estimated wall temperature increases sharply after 9,676sec, causing the failure of the reactor pressure vessel at 14,271sec. The temperature change is enormous from 425K to 1358K within 500sec, causing a reactor failure. The *dT* plot (Fig. 18(b)) has a negative slope in the beginning and then a positive slope after 5,462sec. Furthermore, the *dT* curve has a negative slope at 6,018sec, and then a big positive spike is noticed corresponding to a huge jump in wall temperatures after 9,676sec (Fig. 18(b)). In both cases, IMM has a better estimation of temperature as compared to KF. In both HS-TEMP.2,000,404 and COR-TLH.301, for LBLOCA, due to the rapid decrease in wall temperature, it is difficult to find out the time of dryout of cooling water. However, we suppose the core relocation is initiated when the estimated wall temperature of the lower hemisphere data point COR-TLH.301 increases around 5,462sec.

All the seven data points for *T* and *dT* of the LBLOCA scenario are plotted in Fig. 19. And, the lower hemisphere data points have high wall temperature values as compared to the data points on the reactor core. The sequence of events in the LBLOCA scenario, such as cooling water injection, and core relocation for the bottom hemisphere data point COR-TLH.101 (yellow) is predicted before as compared to the data points on the reactor core and upper plenum (Fig. 19).

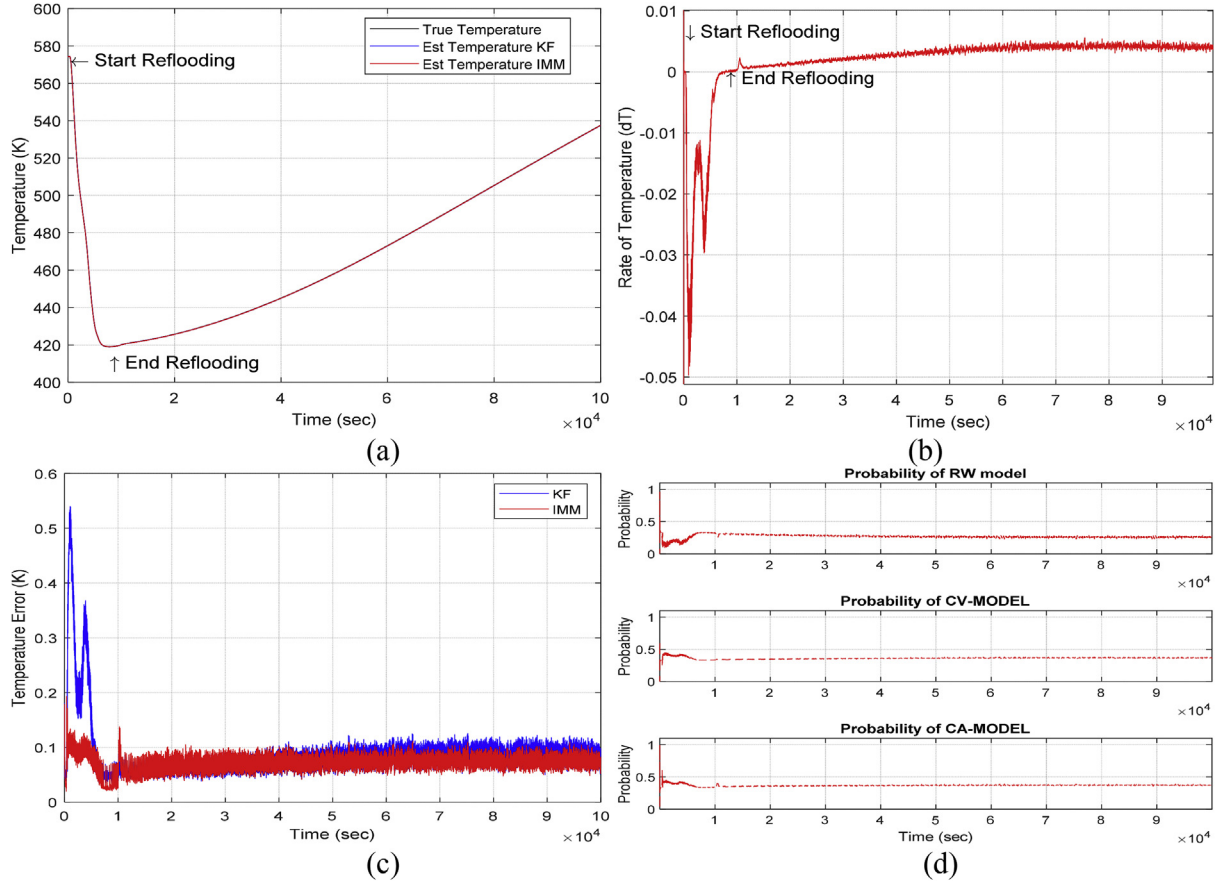

Fig. 17. Results for wall temperature estimation in LBLOCA scenario for data point 4 (HS-TEMP.2,000,404) (a) estimated outer wall temperature using KF and IMM (b) estimated rate of temperature with IMM (c) temperature estimation error (d) model probabilities.

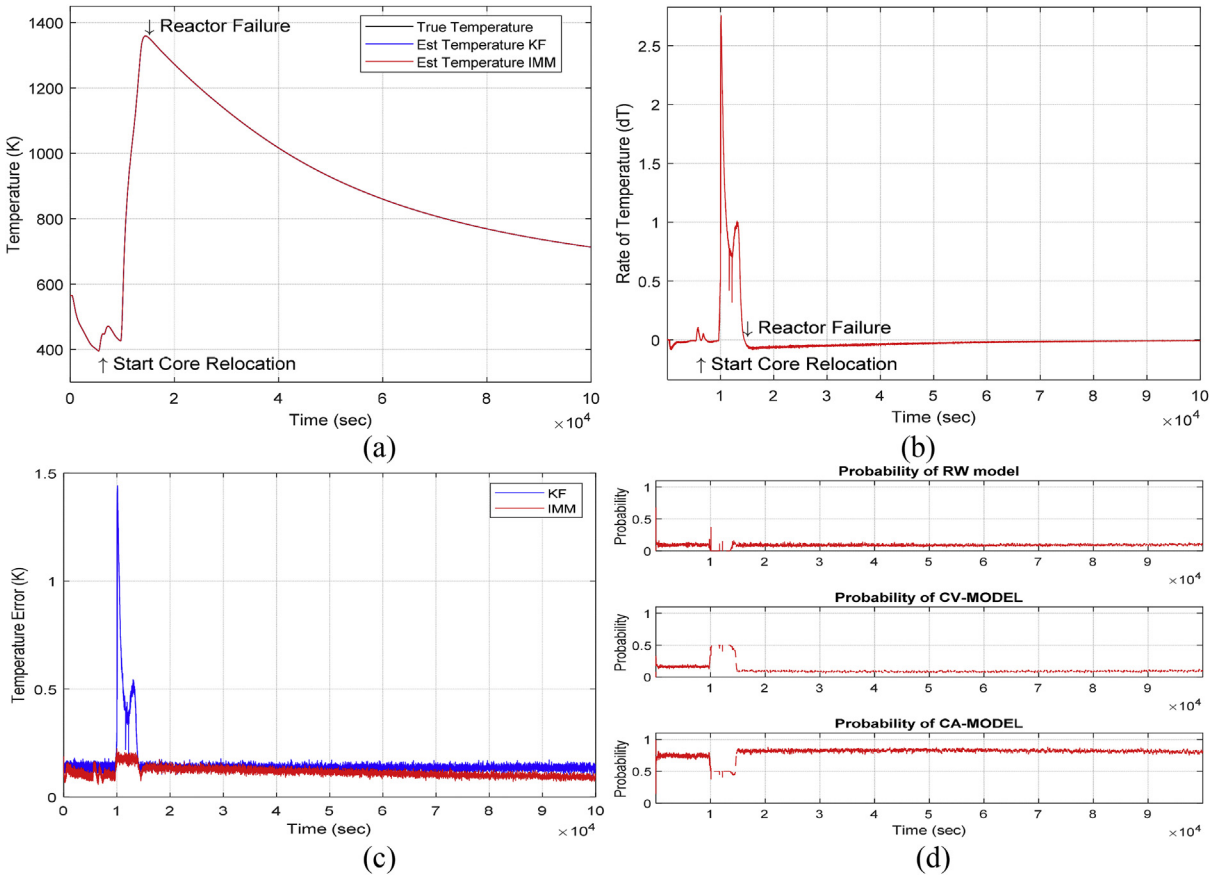

Fig. 18. Results for wall temperature estimation in LBLOCA scenario for data point 6 (COR-TLH.301) (a) estimated outer wall temperature using KF and IMM (b) estimated rate of temperature with IMM (c) temperature estimation error (d) model probabilities.

5. Conclusions

An algorithm based on IMM is developed for the identification of in-vessel phenomena during a severe accident. Identification is done from the estimated out-wall temperature measurement recorded outside of the RV. Multiple models using random-walk, constant velocity, and constant acceleration are used to describe the evolution of transient temperature. The estimated wall temperature and the rate of temperature using IMM are used to identify the in-vessel phenomena during the progression of SA. The sequence of the in-vessel phenomenon is classified as core dryout, corium relocation, reflooding, and reactor failure. IMM using multiple models has a better estimation of wall temperature as compared to KF using a single model. Based on the results, it is found that when the temperature fluctuation is small and random then the random-walk model is dominant as compared to the CA

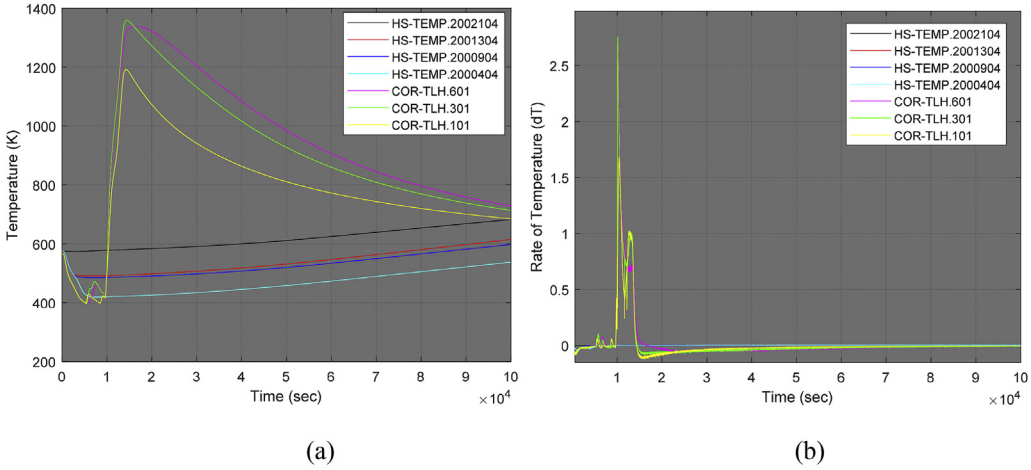

Fig. 19. Results for wall temperature estimation at all seven data points in LBLOCA scenario (a) estimated outer wall temperature using IMM at different locations of the reactor (b) estimated rate of temperature.

and CV model. Furthermore, if the temperature drop or increase is abrupt then the CA model is observed to be dominant. And, if the temperature change is steady, and has a linear or nonlinear behavior, a combination of CA and CV model are dominant as compared to the random-walk model. Therefore, the time of core dryout and core relocation are identified clearly at an early stage of SA by using the CA and CV models. Model probabilities are evaluated for each of the three temperature models, and the weighted estimate based on the evaluated model probabilities is used as a final estimate for wall temperature estimation. An application of a modified IMM based FDD model is useful to classify and identify in-vessel events arising after the SA by using the out-wall temperature of the RV.

Unlike the core components, there is no significant change in the estimated axial temperature on the outer wall, depending on the severe accident scenarios. However, it can be noticed that there is an increase in the wall temperature due to core depletion, and when the safety injection water is injected during the damage of the reactor pressure vessel, the wall temperature is found to decrease. The slope of the temperature curve varies according to the rate of change of wall temperature. Similar to the cylindrical exterior wall, the temperature variation on the upper head exterior wall is not as large as the temperature across the core components. However, as with the cylindrical exterior wall temperature, the estimated wall temperature on the lower bottom hemisphere increases after the core depletion, reactor pressure vessel damage, and decreases with the introduction of safety injection water. Also, the sequence of in-vessel phenomena such as dryout, corium relocation, cooling water injection, reflooding appears before for the bottom hemisphere data points as compared to the data points on reactor core and upper plenum.

An application and installation of measurement of the out-wall temperature of the RV should be considered carefully, because of the insulation material on the exterior wall of RV. However, there is no problem to tightly bend TC (thermocouple) on the exterior wall of RV.

In future work, the practical application for monitoring of in-vessel phenomena during a severe accident using the measurement of the out-wall temperature can be considered to integrate model-based FDD methods with the data-driven methods such as CNN, RNN, neural network, etc which use the extracted features from the random-walk model, CA and CV model.

Declaration of competing interest

The authors declare that they have no known competing financial interests or personal relationships that could have appeared to influence the work reported in this paper.

Acknowledgments

This work was supported by the National Research Foundation of Korea (NRF) grant funded by the Korean government (MSIT: Ministry of Science and ICT) (No. 2017M2A8A4017932). This research was also supported by the 2019 scientific promotion program funded by Jeju National University.

References

[1] A. Suthar, M. Kumar, Critical accident scenario analysis of pressurized water reactor, in: ICTEA: International Conference on Thermal Engineering May 7, 2019.
[2] X. Gaus-Liu, G. Albrecht, T. Cron, B. Fluhrer, J. Foit, H. Madakoro, R. Stängle, M. Vervoortz, T. Wenz, Analysis of Severe Accidents, Annual Report 2017-2018 of the Institute for Nuclear and Energy Technologies (KIT Scientific Reports; 7756), vol. 7756, 2019, pp. 29–36.
[3] J.J. Herbst, R.G. Sider, R.E. Jaquith, C.H. Meijer, Nuclear Plant Safety Evaluation System, Combustion Engineering Inc, 1986. U.S. Patent 4,632,802.
[4] S.G. Kim, Y.G. No, P.H. Seong, Prediction of severe accident occurrence time using support vector machines, Nuclear Engineering and Technology 47 (2015) 74–84.
[5] M.G. Na, S.H. Shin, S.M. Lee, D.W. Jung, S.P. Kim, J.H. Jeong, B.C. Lee, Prediction of major transient scenarios for severe accidents of nuclear power plants, IEEE Trans. Nucl. Sci. 51 (2004) 313–321.
[6] Y.G. No, J.H. Kim, M.G. Na, D.H. Lim, K.I. Ahn, Monitoring severe accidents using AI techniques, Nuclear Engineering and Technology 44 (2012) 393–404.
[7] D. Miljković, Fault detection methods: a literature survey, in: 2011 Proceedings of the 34th International Convention MIPRO, Opatija, May 23, 2011.
[8] S.S. Tayarani-Bathaie, Z.N.S. Vanini, K. Khorasani, Dynamic neural network-based fault diagnosis of gas turbine engines, Neurocomputing 125 (2014) 153–165.
[9] D. Zhang, Q.G. Wang, L. Yu, H. Song, Fuzzy-model-based fault detection for a class of nonlinear systems with networked measurements, IEEE Trans Instrum Meas 62 (2013) 3148–3159.
[10] J. Chen, C. Roberts, P. Weston, Fault detection and diagnosis for railway track circuits using neuro-fuzzy systems, Contr. Eng. Pract. 16 (2008) 585–596.
[11] B. Fan, Z. Du, X. Jin, X. Yang, Y. Guo, A hybrid FDD strategy for local system of AHU based on artificial neural network and wavelet analysis, Build. Environ. 45 (2010) 2698–2708.
[12] J.C.M. Oliveira, K.V. Pontes, I. Sartori, M. Embiruçu, Fault detection and diagnosis in dynamic systems using weightless neural networks, Expert Syst. Appl. 84 (2017) 200–219.
[13] F. Jia, Y. Lei, L. Guo, J. Lin, S. Xing, A neural network constructed by deep learning technique and its application to intelligent fault diagnosis of machines, Neurocomputing 272 (2017) 619–628.
[14] Y. Liu, W. Ni, Z. Ge, Fuzzy decision fusion system for fault classification with analytic hierarchy process approach, Chemometr. Intell. Lab. Syst. 166 (2017) 61–68.
[15] B. Özyurt, A. Kandel, A hybrid hierarchical neural network-fuzzy expert system approach to chemical process fault diagnosis, Fuzzy Set Syst. 83 (1996) 11–25.
[16] C.K. Lau, K. Ghosh, M.A. Hussain, C.C. Hassan, Fault diagnosis of Tennessee Eastman process with multi-scale PCA and ANFIS, Chemometr. Intell. Lab. Syst. 120 (2013) 1–14.
[17] I.S. Lee, J.T. Kim, J.W. Lee, D.Y. Lee, K.Y. Kim, Model-based fault detection and isolation method using ART2 neural network, Int. J. Intell. Syst. 18 (2003) 1087–1100.
[18] Y. Bar-Shalom, X.R. Li, Estimation and Tracking: Principles, Techniques and Softwares, Artech House, Inc, Norwood, MA, 1993.
[19] X.R. Li, Y. Zhang, Multiple model estimation with variable structure, IEEE Trans. Automat. Contr. 41 (1996) 478–493.
[20] B.S. Kim, U.Z. Ijaz, J.H. Kim, M.C. Kim, S. Kim, K.Y. Kim, Nonstationary phase boundary estimation in electrical impedance tomography based on the interacting multiple model scheme, Meas. Sci. Technol. 18 (2006) 62.
[21] M.J. Peng, H. Wang, S.S. Chen, G.L. Xia, Y.K. Liu, X. Yang, A. Ayodeji, An intelligent hybrid methodology of on-line system-level fault diagnosis for nuclear power plant, Nuclear Engineering and Technology 50 (2018) 396–410.
[22] Z. Zhang, J. Chen, Fault detection and diagnosis based on particle filters combined with interactive multiple-model estimation in dynamic process systems, ISA Trans. 85 (2019) 247–261.
[23] S.M. Kargar, K. Salahshoor, M.J. Yazdanpanah, Integrated nonlinear model predictive fault tolerant control and multiple model based fault detection and diagnosis, Chem. Eng. Res. Des. 92 (2014) 340–349.
[24] B. Pourbabaee, N. Meskin, K. Khorasani, Multiple-model based sensor fault diagnosis using hybrid Kalman filter approach for nonlinear gas turbine engines, in: 2013 American Control Conference (ACC), Washington, DC, USA, June 17-19, 2013.
[25] T. Hsiao, M.C. Weng, A hierarchical multiple-model approach for detection and isolation of robotic actuator faults, Robot. Autonom. Syst. 60 (2012) 154–166.
[26] A. Gelb, Applied Optimal Estimation, MIT Press, 1974.
[27] A.K. Khambampati, A. Rashid, U.Z. Ijaz, S. Kim, M. Soleimani, K.Y. Kim, Unscented Kalman filter approach to tracking a moving interfacial boundary in sedimentation processes using three-dimensional electrical impedance tomography, Phil. Trans. Math. Phys. Eng. Sci. 367 (2009) 3095–3120.
[28] B.S. Kim, M.C. Kim, S. Kim, K.Y. Kim, Nonstationary electrical impedance tomography with the interacting multiple model scheme, Meas. Sci. Technol. 15 (2004) 2113.
[29] K.Y. Kim, B.S. Kim, M.C. Kim, S. Kim, D. Isaacson, J.C. Newell, Dynamic electrical impedance imaging with the interacting multiple model scheme, Physiol. Meas. 26 (2005) S217.
[30] Y.J. Kim, W.J. Choi, S.J. Kim, Efficacy assessment of independent severe accident mitigation measures in OPR1000 using MELCOR code, J. Nucl. Sci. Technol. 54 (2017) 89–100.